ISSN 0001-4338, Izvestiya, Atmospheric and Oceanic Physics, 2019, Vol. 55, No. 6, pp. 640–649. © Pleiades Publishing, Ltd., 2019.
Russian Text © The Author(s), 2019, published in Izvestiya Rossiiskoi Akademii Nauk, Fizika Atmosfery i Okeana, 2019, Vol. 55, No. 6.

Mechanism of a Positive Feedback in Long-Term Variations of the Convergence of Oceanic and Atmospheric Heat Fluxes and of the Ice Cover in the Barents Sea

K. A. Kalavichchi[a, *] and I. L. Bashmachnikov[a, b, **]

[a] *St. Petersburg State University, St. Petersburg, 199034 Russia*
[b] *Nansen International Environmental and Remote Sensing Centre, St. Petersburg, 199034 Russia*
**e-mail: katrina.calavicci@mail.ru*
***e-mail: igorb1969@mail.ru*

Received March 16, 2019; revised June 24, 2019; accepted August 7, 2019

Abstract—This paper presents the results of a study of the interannual variability of the convergence of oceanic and atmospheric advective heat fluxes in the Barents Sea region for 1993–2014 using combined (in situ, satellite, and model-based) datasets: ARMOR-3D and ERA-Interim. The convergence of oceanic and atmospheric heat fluxes play a leading role in variations of the area of ice cover of the Barents Sea on interdecadal and interannual time scales, respectively. The interdecadal and the interannual variations of the oceanic heat flux are mainly shaped by current velocity variations in the western boundary of the Barents Sea. The contribution of current velocity to interdecadal variations is 70% of the increase in the oceanic heat flux, mainly due to an increased transport in the North Cape Current. The variations in the transport of the North Cape and of the Return currents has been found to be associated with the variation in the meridional gradient of the zonal wind speed, which, in turn, is caused by an increased oceanic heat transport into the Barents Sea and by the resulting melting of the sea ice. The in situ observations confirm the possible efficiency of the positive feedback between variations in the oceanic heat flux into the Barents Sea, the area of the ice cover, and of the character of atmospheric circulation in the Barents Sea region on decadal time scales.

Keywords: the Barents Sea, the Arctic, ARMOR, ERA-Interim, oceanic heat flux, atmospheric heat flux, ice cover

DOI: 10.1134/S0001433819060173

INTRODUCTION

Since the early 21st century, there has been a slowdown in the increase in average annual near-surface air temperature in the Northern Hemisphere; however, the temperature continues to increase at the same rate [1], which is associated with a decrease in the Arctic sea-ice extent [2, 3]. Consistently, the reduction in the sea-ice extent in the Barents Sea in recent decades is maximal in the Arctic region [2, 4]. The heat transferred by the ocean and the atmosphere to the Barents Sea region can be a significant factor of this "Arctic intensification." Advective heat fluxes govern ice conditions in the Barents Sea and affect the climate of the entire Eurasian sector of the Arctic [5, 6]. The change in heat flux from the ocean to the atmosphere caused by the reduction of the sea-ice extent in the Barents Sea may be the origin of large-scale variability of atmospheric circulation [7, 8].

At present, there is no consensus on the magnitude of the relative contribution of oceanic and atmospheric heat fluxes to the ongoing reduction in the sea-ice extent. Some authors suggest that the main contribution is formed by the oceanic heat advection [9], while others believe that the interannual variability in the sea-ice extent is largely affected by atmospheric circulation [10]. However, the atmosphere affects the heat balance of the Barents Sea not only through the advected heat. Atmospheric circulation largely determines the rate of the oceanic heat flux through the Barents Sea Opening [11]. In turn, the oceanic heat flux amplifies the westerly winds in the southwestern part of the sea, which leads to a further increase in the oceanic heat influx. The efficiency of this positive feedback proposed in [12] from an analysis of a coupled ocean–atmosphere model is examined in this paper using in situ observations.

DATA AND METHODS

This paper analyzes interannual variability of convergence of oceanic and atmospheric heat fluxes from 1993 to 2014.

Advection of atmospheric heat fluxes through the boundaries of the research domain (Fig. 1) was esti-

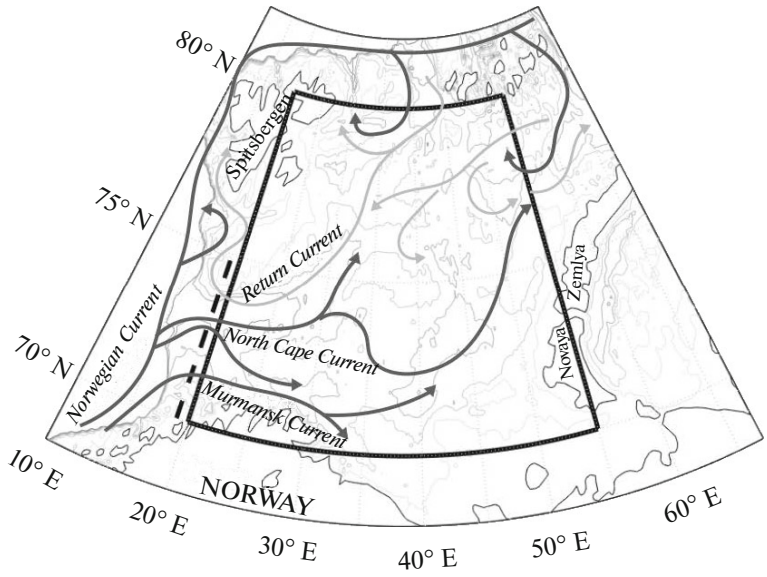

Fig. 1. Bathymetry of the study domain. Thick black lines show the sections through which atmospheric (solid lines) and oceanic (dashed lines) heat fluxes were computed. Black arrows show the currents transporting the Atlantic water and gray arrows show the currents transporting the Arctic water.

mated using air temperature and wind speed from ERA-Interim analysis (http://apps.ecmwf.int/datasets) with the spatial resolution of 0.75 degrees and the temporal resolution of 6 h.

Atmospheric heat fluxes through the boundaries of the Barents Sea were computed using the formula $Q_A = T_a v_a \rho_a C_{pa} dz dx$, where T_a is air temperature (K); v_a is the wind speed (m s^{-1}); $\rho_в = \frac{p_d}{R_d t_a} + \frac{p_v}{R_v t_a}$ – is air density (kg m^{-3}); $C_{pa} = 1005$ J kg^{-1} K^{-1} is the specific heat of air; dz is the cell height (m); dx is the horizontal cell scale (m), p_d and p_v are the partial pressures, and R_d and R_v are the specific gas constants of dry air and water vapor, respectively.

The vertical profiles of atmospheric heat fluxes averaged over the period from 1993 to 2014 and from 1000 to 100 hPa (Figs. 2a, 2b), are similar for zonal and meridional boundaries, respectively. The meridional fluxes at different heights corresponds to earlier obtained values of meridional heat transfer through 70° N [13, 14].

The convergence of atmospheric heat advection was calculated by summing the difference in heat fluxes through the western and eastern and southern and northern boundaries of the Barents Sea. The variability of the horizontal convergence of atmospheric heat fluxes in the lower troposphere was analyzed from 1000 to 850 hPa (Fig. 2c).

The oceanic heat fluxes were computed using ARMOR-3D data (http://marine.copernicus.eu), providing four-dimensional fields of water temperature and current velocity on a regular grid with the spatial resolution of 0.25 degrees at standard oceanographic levels and with temporal resolution of 1 month since 1993. The final fields were obtained through the combination of field and satellite observations. The in situ vertical profiles of temperature and salinity were obtained by CTD profilers, ARGO buoys, and XBT bathothermographs. Satellite observations include satellite altimetry (AVISO, https://www.aviso.altimetry.fr) and ocean surface temperature (Reynolds SST, https://www.nhc.noaa.gov/sst/). The data array also uses surface current velocity data obtained from surface drifting buoys.

Data on temperature and salinity in the regular grid are obtained in two stages. First, at each point, "synthetic" profiles are constructed from the earlier obtained relationships between temperature (or salinity) at different levels and anomalies of ocean surface temperature and sea level obtained from satellite data. Then, the method of optimal interpolation is used to interpolate the "synthetic" and in situ profiles with different weights to the regular grid. The currents at the sea surface are obtained from satellite altimetry and drifters, and the currents at standard levels are obtained by extrapolating surface geostrophic currents into the ocean using the thermal wind relationships and information on water density. The latter is obtained from the previously gridded temperature and salinity fields.

The use of satellite information (with a high spatial and temporal resolution) and episodic in situ observations of high accuracy results in a more robust estimate for the spatial and temporal variability of ocean characteristics than if using in situ observations only. These advantages of the data array are especially evident for

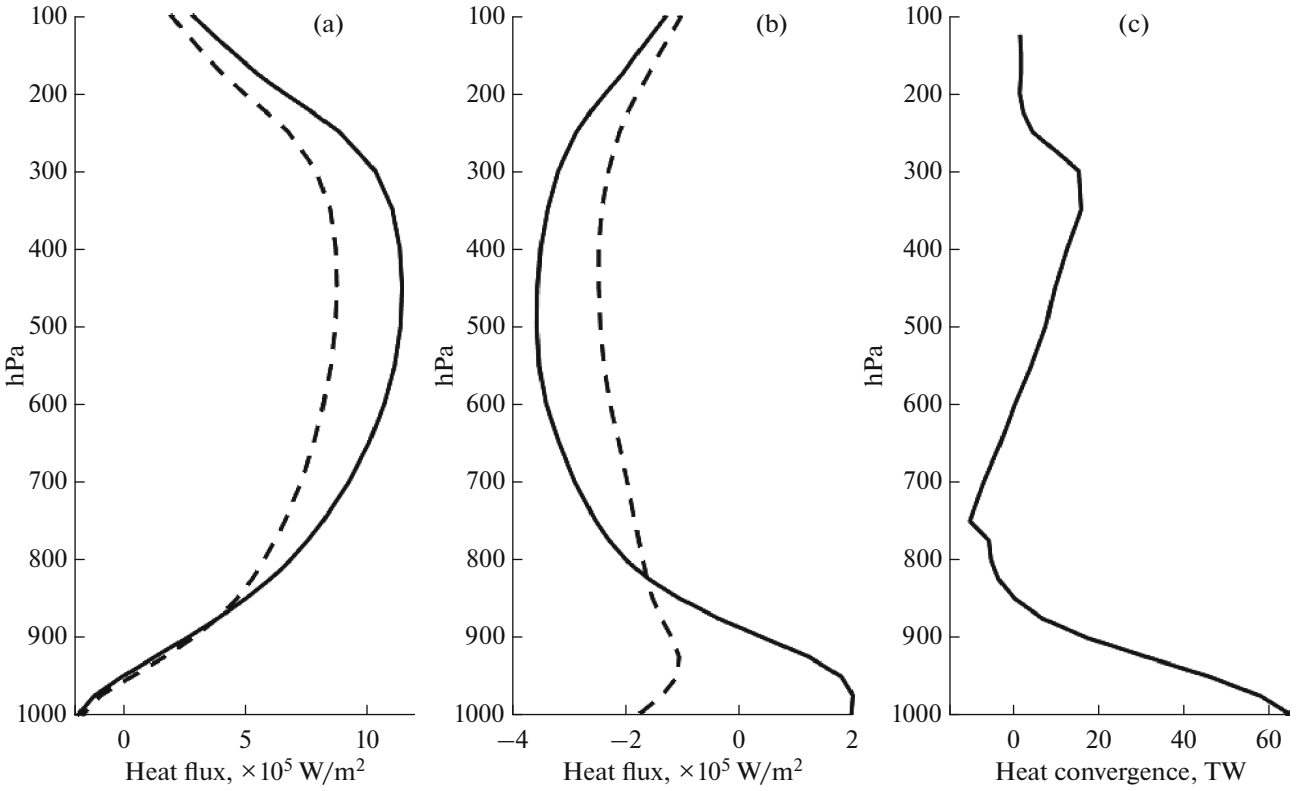

Fig. 2. Vertical sections of averaged (over 1993–2014) atmospheric heat fluxes (W m^{-2}): (a) zonal—through the western (solid line) and eastern (dashed line) boundaries and (b) meridional—through the southern (solid line) and northern (dashed line) boundaries of the Barents Sea (see Fig. 1); the positive heat fluxes are eastward and northward, respectively. (c) Vertical profile of average integral atmospheric heat flux convergence through the Barents Sea boundaries (TW).

shallow-water regions, such as the Barents Sea Opening, with a significant barotropic component of the flow.

The oceanic heat flux across the western boundary of the sea (Fig. 1.) was computed as: $Q_O = (T - T_b)V\rho C_p dzdx$, where T is the water temperature (°C), $T_b = -1.8$°C is the "reference temperature" (the seawater freezing temperature), V is the current velocity (m s^{-1}), $\rho = 1030$ kg m^{-3} is water density, and $C_p = 4183$ J kg^{-1} C^{-1} is the specific heat of water.

The oceanic heat flux was computed through the western boundary of the Barents Sea, between the northern boundary of Norway and the Bear Island. In previous studies, the heat influx into the Barents Sea through this section was estimated at around 50 TW (at $T_b = 0$°C) [15, 16]. The amount of heat transferred to the Barents Sea through the northern boundary of the sea is an order of magnitude smaller: ~1 (+/–5) TW [15, 17]. The presence of ice in the northern and eastern parts of the sea makes it difficult to obtain reliable flux estimates in these regions. The oceanic heat fluxes through the northern and the eastern boundaries were not used in this study. The almost lack of observations would induce an error in the results, rather than improve their accuracy. Thus, the variability in convergence of the oceanic heat flux is a function only of variability of the oceanic heat flux at the western boundary of the sea.

The area of ice cover in the Barents Sea was computed with a temporal resolution of 1 month and a spatial resolution of 0.25 degrees using ERA-Interim reanalysis data (http://apps.ecmwf.int/datasets).

RESULTS

1. Interannual Variability of the Convergence of Oceanic and Atmospheric Heat Fluxes in the Barents Sea

In addition to the average annual values, we also assess the interannual variability of the parameters for five seasons, selected to account for the phases of the seasonal ice variations in the Barents Sea: January–March (stable ice cover), April (maximum ice cover), May–August (active ice melting), September (minimum ice cover), and October–December (active ice formation) [11, 18].

Table 1 presents statistics on the convergence of oceanic and atmospheric (in the layer of 1000–850 hPa) heat fluxes. Atmospheric heat fluxes include both advective as well as eddy heat fluxes. The average oce-

Table 1. Characteristics of convergence of integral oceanic and atmospheric heat fluxes through the boundary of the Barents Sea (TW). RMS is the root-mean square error, *Cv* is the coefficient of variation, and *a* is the angular coefficient of the linear trend (the critical values for significant trends are given in parentheses)

	January–March	April	May–August	September	October–December	Year
Oceanic heat flux						
Average, TW	123	83	79	98	124	102
RMS error, TW	22	21	14	27	23	16
C_v, %	18	25	18	28	18	16
a, TW/year	0.9(0.4)	1.5(0.4)	1.5(0.3)	2.5(0.6)	2.7(0.5)	2.0(0.3)
Convergence of atmospheric heat fluxes						
Average, TW	405	263	4	217	336	225
RMS error, TW	283	207	96	209	158	102
C_v, %	70	79	2400	1174	96	45
a, TW/year	−16(6)	7 (4)	−4(2)	1(4)	−1(3)	−5(2)

anic heat flux over the entire study period was 102 TW. Earlier estimates of the average oceanic heat flux in a section located 35 km to the east at the same T_b was 78 TW, performed using the Massachusetts Institute of Technology General Circulation Model (MIT GCM) [19]. The maximum values of the oceanic heat flux are reached during the cold season (October–December and January–March), which is typical for this region [11].

Over the observation period, linear trends were computed over the annual and the seasonal mean convergence of the oceanic and the atmospheric heat in the study region (Figs. 3a, 3b). The confidence intervals of the angular coefficients of linear trends were computed as [20]: $b_1 \pm \frac{(S_y t_{95,N-1})}{(N-1)^{1/2} S_x}$, where $t_{95,N-1}$ is the value of Student's distribution at a significance level of 95% and $N-1$ degrees of freedom, where N is the length of the time series; $s_y = \left[\frac{1}{N-2}\sum_{i=1}^{N}(y_i - \hat{y}_i)^2\right]^{1/2}$, $s_x = \left[\frac{1}{N-1}\sum_{i=1}^{N}(x_i - \bar{x})^2\right]^{1/2}$, y_i and $\hat{y}_i$ stand for the original series and the linear trend at the data-points x_i, and $\bar{x}$ is the average value of x_i.

The results indicate a significant steady increase in the heat transport of almost 2 TW per year over the observation period (Fig. 3a). The angular coefficients of the trend are significant for annual, as well as for seasonal mean values (Table 1). Earlier calculations using the MIT model for 1993–2014 revealed an increase in the oceanic heat flux by 1 TW per year [19], and the field data for 1998–2006 yielded 2.5 TW per year [16].

The average convergence of atmospheric heat fluxes over the whole study period was 225 TW. The maximum (by magnitude) values of heat convergence are observed in the cold period (October–December and January–March). The standard deviation and the coefficient of variation of the convergence of atmospheric heat fluxes are significantly higher than for the oceanic ones. The linear trends show a tendency towards a decrease in the atmospheric heat convergence since 1993 (Fig. 3b) for the whole year and almost all seasons except April and September (Table 1). Other studies also noted some weakening of the meridional atmospheric heat transfer to the Arctic region during recent decades [13, 17] (see Table 1 and Fig. 3b).

This analysis allows us to assume a leading role of the convergence of the oceanic heat flux in the interdecadal variability of the sea-ice extent in the Barents Sea.

2. Mechanisms of Interdecadal Variability of the Oceanic Heat Flux into the Barents Sea

The increase in the oceanic heat transport, derived in the previous section can be associated with both an increase in water temperature and in current velocity. According to ARMOR-3D data, the average water temperature over the section (1993–2014) was 5.9°C and the average current velocity over the section was 2.8 cm s^{-1} (Figs. 4a, 4b). In the Barents Sea Opening (Fig. 4b), the warm Murmansk Current and two branches of the North Cape Current lie south of the cold Return Current identified in the northernmost part of the section [16].

Positive trends were observed both in the average annual values of the current velocity and in the average annual values of water temperature (Figs. 5a, 5b). This is confirmed by the earlier in situ observations [11, 16]. Knowing the initial and final (along the a linear trend) values of water temperature and of current velocity, one

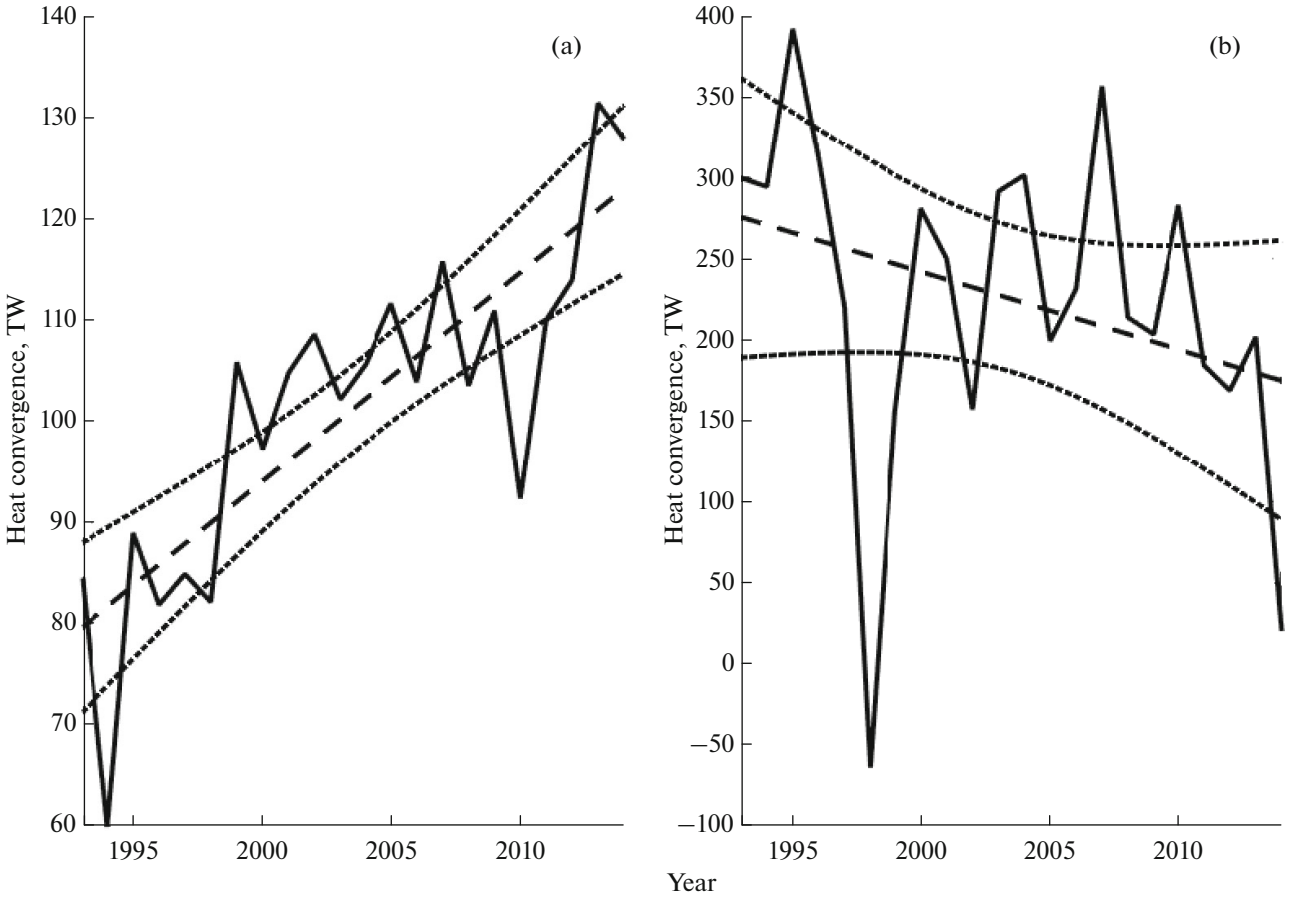

Fig. 3. Interannual variability (annual averaging) of convergence of integral (a) oceanic and (b) atmospheric (1000–850 hPa) heat fluxes through the Barents Sea boundary (solid lines, TW); linear trends (dashed lines) and confidence intervals (dotted lines).

can estimate the contribution of each of these variables to the general trend of the oceanic heat flux as:

$$Q_2 - Q_1 = \rho C_p dz dx \times \left[\frac{1}{2}(T_2 + T_1)(V_2 - V_1) + \frac{1}{2}(V_2 + V_1)(T_2 - T_1)\right], \quad (1)$$

where Q_1 and Q_2 are the initial and final values of heat flux along the trend line, respectively; T_1 and T_2 are the initial and final temperatures along the trend line, respectively; and V_1 and V_2 are the initial and final current velocities along the trend line, respectively. In formula (1), the total linear tendency in the heat flux over the observation period is split among the contribution of the current velocity (the first term of the right-hand side) and the contribution of water temperature (the second term of the right-hand side). These terms are computed at each point of the regular grid with a subsequent integration over the oceanic section.

The calculation using the right-hand side of the formula indicated that the total amount of heat carried by the ocean over the whole study period increased by 40.3 TW, and the growth of the total heat flux according to the left-hand side of the formula was 40.4 TW. The slight discrepancy can be caused by the error from the multiply calculated linear trends at each point of the section. Taking into account the confidence intervals of the angular trend coefficient, the increase in the total heat flux in the Barents Sea is in the range from 35 to 46 TW. The contribution of the current velocity the total oceanic heat flux in the Barents Sea was 28 TW (69%). In view of the confidence intervals of the angular trend coefficient, this contribution is in the range from 23 TW (66%) to 33 TW (72%). The contribution of the water temperature to the total oceanic heat flux in the Barents Sea was 12 TW (31%). In view of the confidence intervals of the angular trend coefficient, this contribution is in the range from 11 TW (34%) to 13 TW (28%). Thus, the leading contribution in the long-term variability of the oceanic heat flux is made by an increase in the current velocity, while the observed temperature increase plays a secondary role.

With trends removed, high significant correlation coefficients between the oceanic heat flux and current velocity (0.8–0.9) are observed, for the annual values, as well as for all seasons except April (Table 2). A leading role variations in water transport in seasonal and in the 2–4 years variability of heat fluxes was noted in [19].

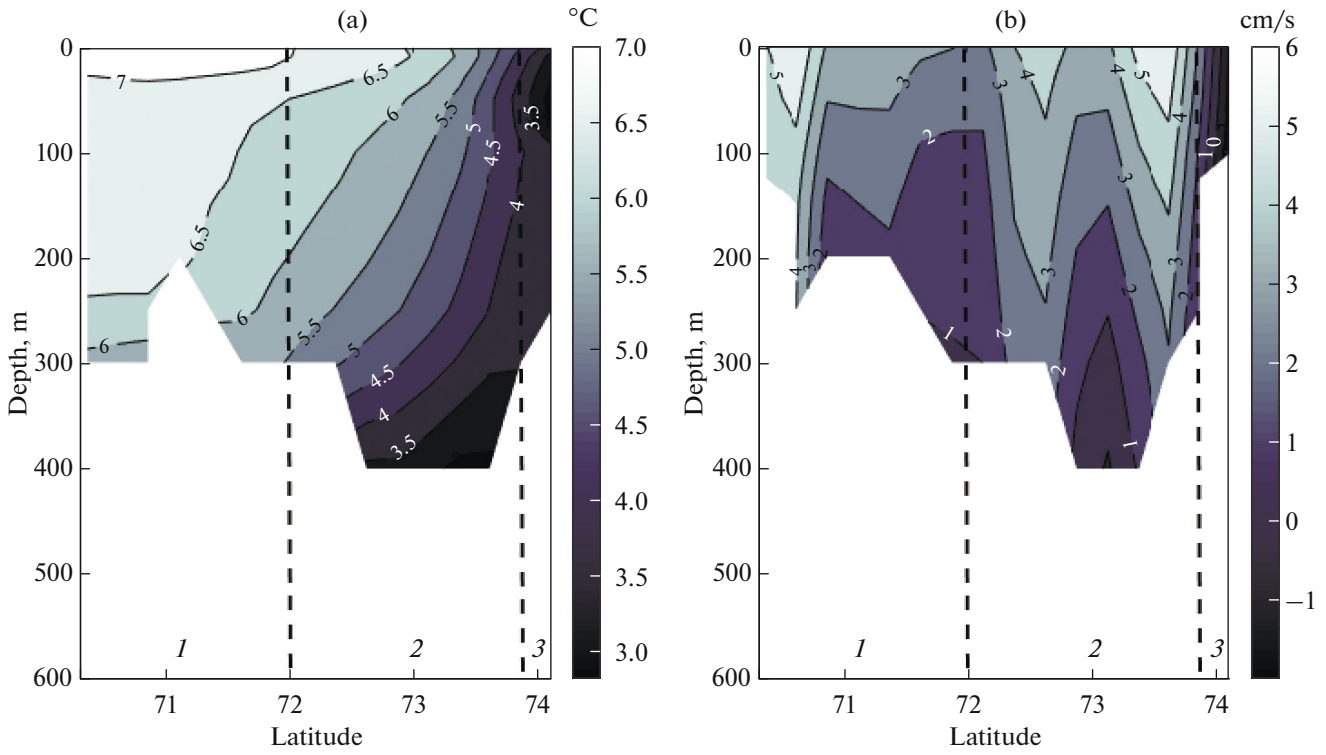

Fig. 4. Vertical sections of water temperature (a) (°C) and of current velocity (b) (cm/s) in the Barents Sea Opening averaged over 1993–2014. Dotted lines indicate the boundaries of the main currents: (*1*) Murmansk, (*2*) North Cape, and (*3*) Return.

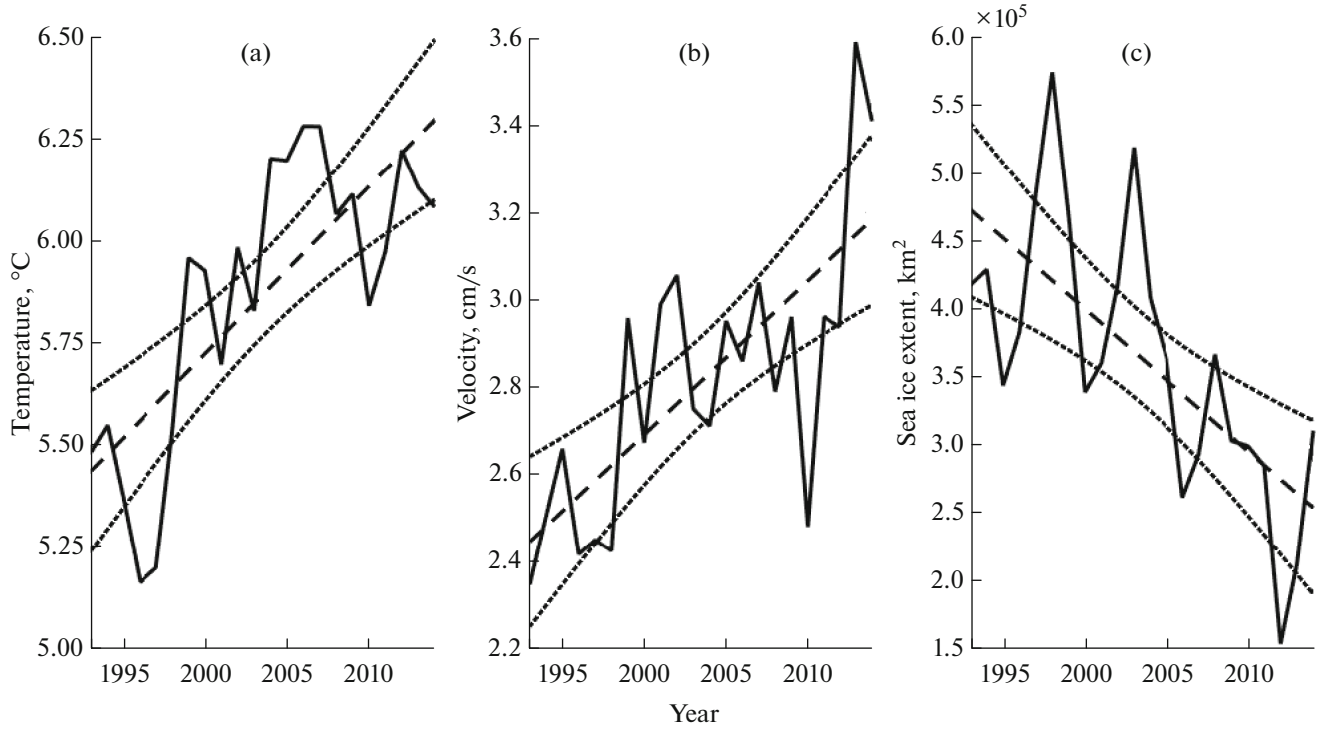

Fig. 5. Interannual variations (annual averaging) of water temperature (a) (°C) and current velocity (b) (cm/s) in the Barents Sea Opening and the area of sea ice in the sea (c) (km^2) (solid lines); linear trends (dashed lines) and confidence intervals (dotted lines).

Table 2. Coefficients of correlation between parameters of the oceanic heat flux in the Barents Sea Opening (the subscript *t* means that the correlations were computed with the linear trends removed; the bold numbers mark coefficients exceeding the 95% significance level), Q_{ot} is the oceanic heat flux, V_t is the current velocity, and T_t is the water temperature

	January–March	April	May–August	September	October–December	Year
Q_{ot} and V_t	**0.94**	0.25	**0.90**	**0.95**	**0.90**	**0.77**
Q_{ot} and T_t	**0.54**	0.25	**0.45**	0.24	0.37	0.38

Table 3. Variations along the trend line (1993–2014) of seasonal and annual mean meridional gradients of the sea level (*gradH*) and of the zonal component of tangential wind stress (*gradW*, N m^{-3}) in the region of the North Cape Current

	January–March	April	May–August	September	October–December	Year
gradH × 10^{-8}	0.2	−8.5	−3.4	−17.8	−16.5	−7.9
gradW × 10^{-9}	33.0	−35.7	3.1	−14.2	−28.7	−2.1

Significant (though low) correlations between the oceanic heat flux and water temperature were obtained only for two seasons: January–March (0.54) and May–August (0.45). The leading role of water transport in the interannual variability of oceanic heat flux into the Barents Sea Opening is consistent with the results obtained in [9].

In summary, our results show that the current velocity is the main factor in the formation of both long-term and interannual variability of the convergence of oceanic heat flux in the Barents Sea. Further analysis shows that among the three main currents in the Barents Sea Opening, the North Cape Current has the major contribution to the observed water transport variability, responsible for 68% of the observed linear increase in the integral water transport, while the contributions of the Murmansk and the Return currents were 17 and 15%, respectively.

3. Role of Wind in the Variability of Oceanic Heat Flux through the Barents Sea Opening

The water transport in the Barents Sea Opening is the sum of the geostrophic and of Ekman currents. The integral (by depth) Ekman transport was computed as [21]: $U_E = \frac{C_w \rho_a W^2}{f_0 \rho_0}$, where C_w is the friction coefficient (1.45×10^{-3}), ρ_a is the air density (1.2 kg m^{-3}), W is the wind speed (ms^{-1}), f_0 is the Coriolis parameter (1.4×10^{-4} s^{-1}), and ρ_0 is the characteristic water density (1028 kg m^{-3}). The meridional component of the wind velocity is obtained from ERA Interim reanalysis. The integral Ekman transport in the Barents Sea Opening, as well as its interannual variability, turned out to be an order of magnitude smaller than the geostrophic transport: on average, 0.2 Sv against 2.8 Sv, respectively. Therefore, further analysis involves only the dynamics of the geostrophic current. The currents in the Barents Sea Opening have a substantial barotropic component [15]. To estimate this component, we used AVISO satellite altimetry and calculate the interannual variability of the meridional gradient of the sea-level and the current velocity: $U = -\frac{g}{f_0}\frac{\partial \zeta}{\partial y}$, where ζ is the sea level (m) and g is the acceleration of gravity. The section under consideration was divided into three segments corresponding to the average position of the three main currents: Murmansk, North Cape, and Return (Figs. 1, 4b).

In annual means, positive trends in the absolute values of the meridional sea-level gradient are observed only in the region of the North Cape Current, which indicates an intensification of the barotropic component of the current since 1993 (Fig. 6a). The maximum change in the sea-level gradient along the linear trend for 1993–2014 are achieved in April, September, and October–December (Table 3), and are several times higher than the values obtained for other seasons. In the regions of the Murmansk and the Return currents, the linear trends show a decrease of the meridional sea-level gradients in time, which indicates a decrease in the corresponding flows (Fig. 6a). The positive increment in the southern part of the Return Current is associated with a change in the flow direction to the east (the Barents Sea) by the end of the observation period.

In [22, 23], it is demonstrated that the variability of water transport in the Barents Sea Opening between the northern part of Norway and the Bear Island largely depends on atmospheric circulation. An increase in the cyclonic circulation in the western part of the Barents Sea is followed by an increase in Ekman transport and a local sea-level rise in the northwestern part of the sea. The resulting meridional pressure gradients increase the volume of the Atlantic Water entering into the Barents Sea due to the weakening of the Return Current [24].

To assess the effect of wind on the sea level variability and the barotropic current velocity in the Barents Sea Opening, we considered temporal variability of

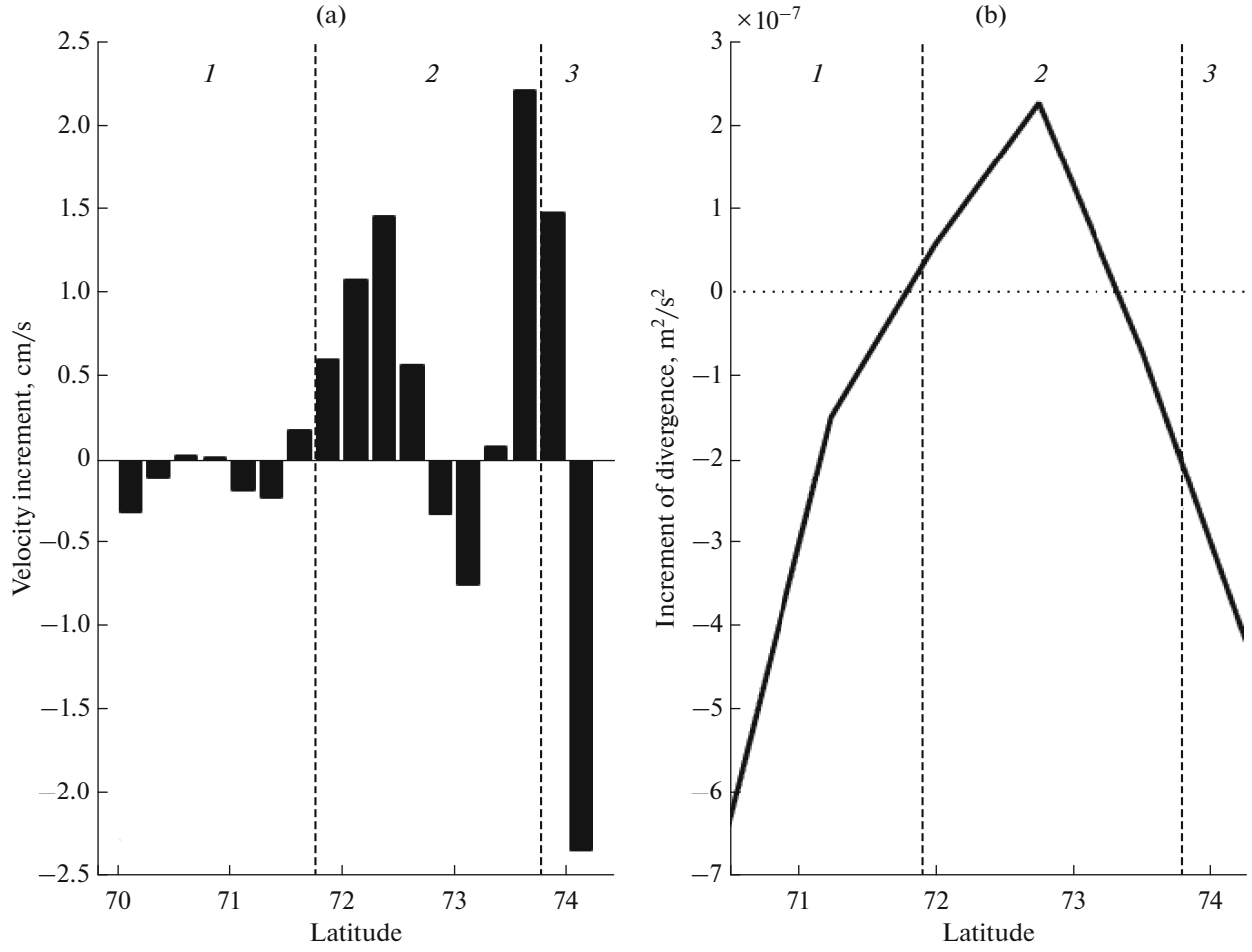

Fig. 6. Increments along the trend lines (1993–2014) of (a) the modulus of current velocity (cm s^{-1}) and (b) the zonal component of the Ekman flux divergence (m^2 s^{-2}) in the Barents Sea Opening. Dotted lines indicate the boundaries of the main currents: (*1*) Murmansk, (*2*) North Cape, and (*3*) Return.

the convergence of the zonal component of Ekman transport along various segments of the given section: $divV = -\frac{\partial}{\partial y}\left(\frac{\tau_x^w}{\rho_0 f_0}\right)$, where τ_x^w is the tangential wind stress (N m^{-2}). An increase in the meridional gradient of the zonal component of the tangential wind stress was observed only in the North Cape Current region. The peak negative values of the angular coefficients of the linear trend in the gradients of the wind stress are observed in September–December and April (Table 3), i.e., during the formation and the maximum sea-ice extent. The resulting increments of the zonal component of Ekman divergence along the section (Fig. 6b), averaged over 1993–2014, are consistent with an increase in the water transport in the North Cape Current and a decrease in the Return Current, both due to the corresponding changes in local sea-level gradients. The weakening of the wind divergence corresponds to some decrease of the velocity in the Murmansk Current; however, the weakening of the coastal current is associated with a local decrease in the wind speed (following a migration of the center of the atmospheric circulation cell), rather than with wind gradient. Thus, the wind-field variability is possibly responsible for the formation of the observed trends: an increase in transport of the North Cape Current and a decrease in transport of the Return Current.

4. The Sea-Ice Extent and the Heat Fluxes in the Barents Sea

The average annual values of the sea ice extent have a pronounced negative trend from 1993 to 2014 (see Fig. 5c and [10, 25]). It was shown in the previous sections that this is a consequence of an increase in the oceanic heat flux to the Barents Sea over the past decades. To assess the role of various factors in governing the short-term interannual variability of the sea ice extent, we computed the correlation coefficients between time series with trends removed (Table 4). Significant negative correlations of the sea ice extent

Table 4. Coefficients of correlation of interannual variations of oceanic and atmospheric parameters with the sea ice extent in the Barents Sea (the subscript t means that the correlations were calculated after linear trends are removed; in bold are the coefficients exceeding the 95% significance level); Q_{ot} is the oceanic heat flux, Q_{at} is the atmospheric heat flux, V_t is the current velocity, and T_t is the water temperature

	January–April	May	June–August	September	October–December	Year
Q_{ot}	**–0.42**	0.16	0.05	–0.02	0.02	0.00
Q_{at}	**–0.52**	–0.09	**–0.44**	0.06	–0.14	**–0.53**
T_t	**–0.42**	**–0.49**	0.10	–0.41	–0.11	–0.04
V_t	**–0.58**	–0.06	–0.05	–0.05	0.09	–0.09

with all the tested parameters were obtained for in the winter period (January–April). The highest correlations were observed between the sea ice extent and the convergence of atmospheric heat fluxes, which indicates the latter to be the main contributor to the interannual variability of the sea ice extent in the Barents Sea in the annual means (Table 4).

CONCLUSIONS

ERA-Interim and ARMOR-3D datasets were used to analyze the average annual and seasonal variability of the convergence of atmospheric and oceanic heat fluxes in the Barents Sea from 1993 to 2014. The seasonal variability is typical for the study region, with the maximum dispersion of the fluxes in winter and minimum in summer. The oceanic flux averaged over the whole study period was 102 TW at $T_b = -1.8$°C, with a positive linear trend of 2 TW per year, which is consistent with previous studies [16, 19]. Significant trends were observed for all seasons. The average atmospheric heat convergence over the study period into the Barents Sea was 225 TW, and the negative linear trends show a decrease in the amount of heat transported by the atmosphere with time. Our results allow us to assume that the oceanic heat flux plays a leading role in the long-term reduction of the sea ice extent in the Barents Sea. However, the convergence of the atmospheric heat fluxes plays the leading role in the interannual variations of the sea ice extent at the smaller interannual time scales.

During the time period considered in this study, almost 70% of the linear increase in the oceanic heat flux in the Barents Sea was due to an increase in the current velocity. The contribution of the increasing water temperature was around 30%. In view of the confidence intervals, the contribution of each of the components varies within 2–4%. At smaller (interannual) time scales, the main contribution of current velocity to the formation of variability of the oceanic heat flux is preserved: the correlation between the oceanic heat flux and the current velocity (averaged over the year and in all seasons) is significant and constitutes 0.77, with almost no correlation with the water temperature.

Further analysis showed the leading role of the variability of the North Cape Current velocity in the interannual variability of the total water transport through the Barents Sea Opening. We obtained a relationship between the variability of the North Cape and Return current velocities with the change in the meridional sea level gradient. The latter is caused by an increase in the convergence of Ekman transport due to the increased gradient of the zonal component of wind velocity in the Barents Sea Opening.

Our analysis confirms the possible efficiency and reveals the details of the positive feedback mechanism proposed earlier on the basis of model results [12]. On interdecadal time scales, a statistical relationship is obtained between an increase in the oceanic heat flux and a decrease in the sea ice extent in the Barents Sea. As a result, the cyclonic atmospheric circulation in the western part of the sea is intensified, which leads to an increase in the gradients of easterly winds in the northwestern part of the sea. No increase in the wind speed in the southwestern part of the Barents Sea and, accordingly, no increase in the Murmansk Current velocity is noted, which contradicts earlier assumptions [26]. The local increase in the meridional gradients of the zonal component of the wind speed results in a stronger heat transport the North Cape Current, while less heat leaves the region with the weakened Return Current. This leads to the further acceleration of the sea ice melt and a further change in the atmospheric circulation.

FUNDING

This study was supported by the Russian Science Foundation, project no. 17-17-01151.

REFERENCES

1. V. A. Semenov, "Influence of oceanic inflow to the Barents Sea on climate variability in the Arctic region," Dokl. Earth Sci. **418** (1), 91–94 (2008).
2. J. A. Screen and I. Simmonds, "The central role of diminishing sea ice in recent Arctic temperature amplification," Nature **464** (7293), 1334–1337 (2010).
3. I. V. Polyakov, L. A. Timokhov, and V. A. Alexeev, et al., "Arctic Ocean warming contributes to reduced

polar ice cap," J. Phys. Oceanogr. **40** (12), 2743–2756 (2010).

4. C. L. Parkinson and D. J. Cavalieri, "Arctic sea ice variability and trends, 1979–2006," J. Geophys. Res: Oceans **113** (C7) C07003 (2008).
5. V. V. Zuev, V. A. Semenov, E. A. Shelekhova, et al., "Evaluation of the impact of oceanic heat transport in the North Atlantic and Barents sea on the Northern Hemispheric climate," Dokl. Earth Sci. **445** (2), 1006–1010 (2012).
6. J. H. Jungclaus and T. Koenigk, "Low-frequency variability of the Arctic climate: The role of oceanic and atmospheric heat transport variations," Clim. Dyn. **34** (2–3), 265–279 (2010).
7. J. Screen and I. Simmonds, "The atmospheric response to three decades of observed Arctic sea ice loss," J. Clim. **26** (4), 1230–1248 (2013).
8. J. Cohen, J. Screen, and J. Furtado, et al., "Recent Arctic amplification and extreme mid-latitude weather," Nat. Geosci. **7** (9), 627–637 (2014).
9. M. Årthun and T. Eldevik, "Quantifying the influence of Atlantic heat on Barents Sea ice variability and retreat," J. Clim. **25** (13), 4763–4743 (2012).
10. S. A. Sorokina, K. Li, and J. J. Wettstein, et al., "Observed atmospheric coupling between Barents Sea ice and the warm-Arctic cold-Siberian anomaly pattern," J. Clim. **29** (2), 495–511 (2016).
11. L. H. Smedsrud, I. Esau, and R. B. Ingvaldsen, et al., "The role of the Barents Sea in the Arctic climate system," Rev. Geophys. **51** (3), 415–449 (2013).
12. L. Bengtsson, V. A. Semenov, and O. M. Johannessen, "The early-twentieth-century warming in the Arctic: A possible mechanism," J. Clim. **17** (20), 4045–4057 (2004).
13. S. A. Sorokina and I. N. Esau, "Meridional energy flux in the Arctic from data of the radiosonde archive IGRA," Izv., Atmos. Ocean. Phys. **47** (5), 572–583 (2011).
14. G. V. Alekseev, S. I. Kuzmina, A. V. Urazgil'deeva, et al., "Influence of the atmospheric heat and moisture transport on Arctic warming in winter," Fundam. Prikl. Klimatol. **1**, 43–63 (2016).
15. L. H. Smedsrud, R. Ingvaldsen, and J. Nilsen, et al., "Heat in the Barents Sea: Transport, storage, and surface fluxes," Ocean Sci. **6** (1), 43–63 (2010).
16. Ø. Skagseth, T. Furevik, and R. Ingvaldsen, et al., "Volume and heat transports to the Arctic Ocean via the Norwegian and Barents seas," in *Arctic–Subarctic Ocean Fluxes* (Springer, Dordrecht, 2008), pp. 45–64.
17. L. H. Smedsrud, A. Sorteberg, and K. Kloster, "Recent and future changes of the Arctic sea-Ice cover," Geophys. Res. Lett. **35** (20), L20503 (2008).
18. E. Mironov, *Ice Conditions in the Greenland and Barents Seas and Their Long-Term Forecast* (AARI, St. Petersburg, 2004) [in Russian].
19. I. L. Bashmachnikov, A. Y. Yurova, L. P. Bobylev, et al., "Seasonal and interannual variations of the heat fluxes in the Barents Sea region," Izv., Atmos. Ocean. Phys. **54** (2), 213–222 (2018).
20. R. E. Thomson and W. J. Emery, *Data Analysis Methods in Physical Oceanography* (Elsevier, Amsterdam, 2014).
21. K. Bowden, *Physical Oceanography of Coastal Waters* (Ellis Harwood, New York, 1984; Mir, Moscow, 1988).
22. R. B. Ingvaldsen, L. Asplin, and H. Loeng, "Velocity field of the western entrance to the Barents Sea," J. Geophys. Res.: Oceans **109** (C3), C03021 (2004).
23. R. B. Ingvaldsen, L. Asplin, and H. Loeng, "The seasonal cycle in the Atlantic transport to the Barents Sea during the years 1997–2001," Cont. Shelf. Res. **24** (9), 1015–1032 (2004).
24. V. S. Lien, P. Schlichtholz, and Ø. Skagseth, et al., "Wind-driven Atlantic water flow as a direct mode for reduced Barents Sea ice cover," J. Clim. **30** (2), 803–812 (2017).
25. N. V. Mikhailova and A. V. Yurovsky, "Analysis of principal components of the sea ice concentration fields in the Barents Sea," Phys. Oceanogr., No. 2, 12–20 (2017).
26. Ø. Skagseth, K. F. Drinkwater, and E. Terrile, "Wind- and buoyancy-induced transport of the Norwegian Coastal Current in the Barents Sea," J. Geophys. Res.: Oceans **116** (C8), C08007 (2011).

Translated by V. Arutyunyan